



Article

Centimeter-Level Orbit Determination of GRACE-C Using IGS-RTS Data

Duoduo Li ^{1,2}, Xuhua Zhou ^{1,*} and Kai Li ¹

¹ Shanghai Astronomical Observatory, Chinese Academy of Sciences, Shanghai 200030, China; liduoduo@shao.ac.cn (D.L.); kli@shao.ac.cn (K.L.)

² School of Astronomy and Space Science, University of Chinese Academy of Sciences, Beijing 100049, China

* Correspondence: xhzhou@shao.ac.cn

Abstract: GNSS real-time applications greatly benefit from the International GNSS Service's (IGS) real-time service (RTS). This service does more than provide for terrestrial precise point positioning (PPP); it also brings more possibilities for space-borne technology. With this service, the State-Space Representation (SSR) product, which includes orbit corrections and clock corrections, is finally available to users. In this paper, the GPS real-time orbit and clock corrections provided by 11 analysis centers (ACs) from the day of the year (DOY) 144 to 153 of 2022 are discussed from 3 perspectives: integrity, continuity, and accuracy. Moreover, actual observation data from the GRACE-C satellite are processed, along with SSR corrections from different ACs. The following can be concluded: (1) In terms of integrity and continuity, the products provided by CNE, ESA, and GMV perform better. (2) CNE, ESA, and WHU are the most accurate, with values of about 5 cm for the satellite orbit and 20 ps for the satellite clock. Additionally, the clock accuracy is related to the Block. Block IIR and Block IIR-M are slightly worse than Block IIF and Block IIIA. (3) The accuracy of post-processing reduced-dynamic precise orbit determination (POD) and kinematic POD are at the centimeter level in radius, and the reduced-dynamic POD is more accurate and robust than the kinematic POD.

Keywords: state-space representation (SSR); space-borne GPS; clock evaluation



Citation: Li, D.; Zhou, X.; Li, K.

Centimeter-Level Orbit

Determination of GRACE-C Using IGS-RTS Data. *Remote Sens.* **2023**, *15*, 1832. <https://doi.org/10.3390/rs15071832>

Academic Editors: Walyeldeem Godah and Mladen Zrinjski

Received: 6 March 2023

Revised: 27 March 2023

Accepted: 28 March 2023

Published: 29 March 2023



Copyright: © 2023 by the authors. Licensee MDPI, Basel, Switzerland. This article is an open access article distributed under the terms and conditions of the Creative Commons Attribution (CC BY) license (<https://creativecommons.org/licenses/by/4.0/>).

1. Introduction

Since the successful implementation of space-borne GPS orbit determination from the Topex/Poseidon [1] altimetry satellite in 1992, many successively launched low earth orbit (LEO) satellites or spacecraft have been equipped with space-borne receivers such as CHAMP [2], JASON [3], GRACE [4], and SENTINEL [5,6]. In recent decades, space-borne technology has been widely used in many fields; this technology greatly relies on precise LEO satellite orbits. The satellite orbits and clocks of the GNSS (Global Navigation Satellite System) are among the most essential prerequisites for LEO precise orbit determination (POD). Centimeter-level LEO position precision can be attained above precise satellite ephemeris [4,7–10]. Unfortunately, the precise ephemeris product has a latency of about two weeks. With the diversification requirements of space-borne missions, a higher request is proposed for the instantaneity of a LEO satellite orbit. In determining the ultra-rapid orbit of LEO satellites using a two-step method, traditional processing methods mainly adopt the products of a rapid satellite precise orbit and precise clock error provided by IGS (or other institutions). Currently, the precision of a satellite orbit in the forecast part of IGS ultra-rapid (IGU) products is 5 cm and the satellite clock bias is 3 ns (about equal to 1 m); the error of the forecast clock bias continuously increases over time, limiting the improvement of LEO POD.

To meet the needs of high-precision real-time positioning, IGS established a real-time working group in 2001. The IGS Real-Time Pilot Project (IGS-RTPP) was launched in 2007 to further expand and refine its existing real-time infrastructure and has provided a real-time service since 1 April 2013 [11–13]. More specifically, the orbit and clock corrections

are estimated in real time using GNSS data collected by the global tracking network. Corrections are then broadcast in the RTCM-SSR (state-space representation) format based on the NTRIP (Network Transport of RTCM over the Internet Protocol) to achieve real-time precise point positioning and related applications on a global scale.

In the past decade, with real-time orbit and clock products becoming more accurate, many international analysis centers (ACs) have provided real-time correction products, including orbit corrections, clock corrections, code biases, phase biases, and atmospheric parameters. The main ACs are the Bundesamt für Kartographie und Geodäsie (BKG), the Institute of Geodesy and Geophysics (IGG) of the Chinese Academy of Sciences (CAS), the Centre National d'Etudes Spatiales (CNES), the Deutsches Zentrum für Luft-und-Raumfahrt (DLR), the European Space Agency (ESA), the German Research Center for Geosciences (GFZ), the Spanish GMV Aerospace and Defense Co.(GMV), Natural Resources Canada (NRCan), the Shanghai Astronomical Observatory (SHAO), and the GNSS Research Center of Wuhan University (WHU). Users can obtain real-time products online through BNC [14], RTKLIB [15], and Net-Diff [16]. Moreover, several commercial companies (such as Fugro's G4 [17], TerraStar-D [18], Hi-Target's Global Precision, and NavCom's Star Fire System [19]) provide paid services, and corrections are broadcast for high-precision real-time positioning. In addition, there are augmentation services embedded in navigation satellite systems, including the QZSS Centimeter-Level Augmentation Service (CLAS) based on the L6E signal [20], the Galileo PPP service based on the E6B signal [21], the BDS GEO PPP-B2b precise point positioning service [22], and the Australia/New Zealand Satellite Augmentation System (AU/NZ-SBAS) [23].

Although a RTS has high-precision terrestrial applications [24–29], it has also been further applied in space-borne technology. Wang et al. [30] simulated an onboard environment to receive real-time RTCM information, including space-borne observations, broadcast ephemeris, and SSR corrections, for kinematic and reduced-dynamic autonomous orbit determinations. Based on the above research, GRACE satellite single-receiver ambiguity fixing was realized through an integer phase clock (IPC) and wide-lane satellite bias (WSB) products from CNES for both kinematic and reduced-dynamic methods [31]. Darugna et al. [6] completed a Sentinel-6A centimeter-level orbit determination based on the GPS/Galileo dual-constellation orbit and clock correction products. It should be noted that complete corrections cannot be received at any time due to the limitations of network delays and communication links. Giordano et al. [32] proposed the concept of multi-antennas to overcome the weak communication links above the poles when receiving corrections from geostationary satellites. Another solution is to predict orbit and clock corrections with high-order polynomials [33]. Hauschild et al. [34] reported that their predicted correction improved the real-time POD of the SWARM-C satellite compared with broadcast ephemeris. Furthermore, real-time orbit and clock corrections may contain large errors or faults, which adversely affect POD. To solve this problem, the orbit and clock are modelled as quasi-observations for fault detection and exclusion, which improves the availability of real-time products [35].

As mentioned above, the current research on SSR products in space-borne technology is mainly aimed at LEO real-time orbit determination. However, most of the current mission requirements for LEO satellites focus on post-processing and near-real-time orbit determination. Additionally, the onboard communication environment is very harsh, and it is difficult to ensure the smooth reception of SSR corrections. In contrast, corrections can be received on the ground within a few seconds or even instantaneously, so they can serve as a substitute for ultra-rapid products to calculate the orbit of the LEO satellite at any observation epoch. Ideally, RTS will be used to achieve ultra-rapid orbit determination for several LEO satellites in the future.

For LEO satellites, there are three main methods for orbit determination: dynamic, kinematic, and reduced-dynamic methods. The kinematic method [36] utilizes onboard GNSS code and carrier-phase tracking data to obtain the LEO satellite orbit and it does not depend on any dynamic model; therefore, the kinematic method is highly dependent on

the high quality of the observations and is more liable to be affected by the visible GNSS satellite constellation, the measurement error, noise, and data interruption. The dynamic method [8] requires rigorous dynamic models to predict the orbit; the model error then accumulates with the increase in the arc length. The reduced-dynamic method [36,37] combines the geometric and dynamic information of the satellite and absorbs the dynamic model error of the unmodeled perturbation error by estimating the empirical parameters and pseudo-random pulse parameters. As it integrates the advantages of the dynamic and kinematic methods, the reduced-dynamic method is the most widely used orbit determination method at present.

This paper proceeds as follows. Section 2 introduces the method whereby real-time satellite orbit and clock products are generated by SSR corrections, and an improved clock error evaluation method is elaborated on. In Section 3, we compare the real-time products of different ACs with IGS post-processing precise products and analyze their integrity, continuity, and accuracy. In Section 4, reduced-dynamic and kinematic orbit determinations of the Gravity Recovery and Climate Experiment (GRACE)-C satellite are carried out. Finally, the main conclusions of this paper are summarized.

2. Methods

2.1. Real-Time Orbit and Clock Recovery

An SSR correction is calculated relative to the broadcast ephemeris. When used, the issue of data parameters in the SSR file is matched with the IODE (Issue of Data, Ephemeris) in the broadcast ephemeris, and the correction with the closest matching time is used as the effective value to recover the precise orbit and clock error.

2.1.1. Real-Time Orbit Recovery

It is assumed that the satellite orbit corrections at time t_0 in RTCM-SSR are defined as $\delta\rho_r$ in radial, $\delta\rho_a$ in along-track, and $\delta\rho_c$ in cross-track directions in the orbit coordinate system, denoted as $\delta = [\delta\rho_r \ \delta\rho_a \ \delta\rho_c]^T$. The orbit correction at time t can then be expressed as:

$$\delta\rho = \delta + \dot{\delta}(t - t_0) \quad (1)$$

where $\dot{\delta}$ is the velocity vector. As the satellite position calculated from the broadcast ephemeris is located in the earth-centered earth-fixed (ECEF) coordinate system, it is necessary to convert the orbit corrections from the coordinate system of the satellite orbit to ECEF. The correction in ECEF $\Delta\mathbf{X} = [\Delta X \ \Delta Y \ \Delta Z]^T$ is computed as:

$$\Delta\mathbf{X} = [\mathbf{e}^r \ \mathbf{e}^a \ \mathbf{e}^c] \delta\rho \quad (2)$$

where $\mathbf{e}^r \ \mathbf{e}^a \ \mathbf{e}^c$ is the unit vector of the satellite orbit coordinate system according to the position and velocity of the satellite in ECEF.

According to the orbit correction vector $\Delta\mathbf{X}$ in ECEF and the satellite position $X_{broadcast}$ calculated by the broadcast ephemeris, the corrected satellite position \mathbf{X} is finally obtained as follows:

$$\mathbf{X} = X_{brdc} - \Delta\mathbf{X} \quad (3)$$

2.1.2. Real-Time Clock Recovery

The clock corrections at time t_0 are characterized as a quadratic polynomial with coefficients C_0 , C_1 , and C_2 . As a result, the satellite clock corrections $C\delta_t$ at time t are as follows:

$$C\delta_t = C_0 + C_1(t - t_0) + C_2(t - t_0)^2 \quad (4)$$

where C is the speed of light in a vacuum. The corrected satellite clock error dt_{Sat} is calculated as follows:

$$dt_{Sat} = dt_{brdc} - \delta_t \quad (5)$$

where dt_{brdc} is the clock error calculated from the broadcast ephemeris.

2.2. Clock Evaluation

In this section, an improved two-times difference (TTD) method is introduced to evaluate the accuracy of the clock error so that we can obtain the clock error accuracy value relative to the reference satellite clock product. When the clock difference is small, it shows that the two clock products have good consistency and a high relative accuracy.

The clock error calculation process is affected by many factors, meaning that each AC refers to a unique bias. To obtain a more accurate relative accuracy of the clock error, it is necessary to unify the coordinate bias and time bias of the clock error.

2.2.1. Coordinate Frame Unification

The satellite orbits adopted in the process of the clock error calculation make a difference to the clock error results. For this reason, compatibility corrections are applied to AC clock solutions prior to the clock comparison to maintain the orbit/clock as well as the reference product consistency [38]. Specifically, the first step is the alignment of the individual AC solution's reference frame to the reference AC, epoch by epoch:

$$\Delta clk_{iepo,AC}^s = ((X_{AC} - X_{REF} - DX) \cdot X_{AC}) / R_{SAT} / C \quad (6)$$

where $\Delta clk_{iepo,AC}^s$ is the consistency correction applied to the AC satellite clock solutions; DX is the origin offset of the AC satellite solutions (X_{AC}), with respect to the reference satellite solutions (X_{REF}); R_{SAT} is the satellite radius vector; and C is the velocity of light in a vacuum.

The influence of the satellite orbit coupling error is deducted for the undifferenced clock error:

$$clk'_{iepo,AC}^s = clk_{iepo,AC}^s - \Delta clk_{iepo,AC}^s \quad (7)$$

where $clk_{iepo,AC}^s$ is the initial undifferenced clock error.

2.2.2. Time Frame Unification

In the second step, the individual AC solutions are aligned to a common reference time frame. The time frame of the satellite clock error is the reference time system of the satellite clock error products. There are differences in the reference stations, reference clocks, and estimation models selected by each AC when calculating the satellite clock error, resulting in different time systems being used for the satellite clock errors calculated by different ACs.

When the traditional TTD method is used to unify the time frame, if the reference satellite is not selected properly, each satellite clock error absorbs the influence of the time frame of the reference satellite, resulting in the same trend for all satellites; this is called a common mode error. In addition, the double difference of each satellite clock error has a systematic bias, which appears as different time series mean values for different satellites; this bias needs to be eliminated in the process of time frame unification.

Two steps are taken to unify the time frame:

1. Trend Error Correction

There is an overall systematic bias for the satellite clock error between the individual AC constellations with the reference AC. Therefore, the center of gravity frame of two ACs is aligned epoch by epoch, effectively eliminating the common mode error between the satellite constellations:

$$clk''_{iepo,AC}^s = clk'_{iepo,AC}^s - \frac{\sum_{s=1}^n (clk'^s_{iepo,AC} - clk'^s_{iepo,REF})}{n} \quad (8)$$

where $clk'_{iepo,AC}$ is the clock error after the orbit/clock compatibility corrections, as detailed in Section 2.2.1; n is the number of effective satellites in the epoch $iepo$, where the outlier in this epoch has been eliminated; and $clk''^s_{iepo,AC}$ is the detrended satellite clock error.

2. Systematic Bias Correction

The systematic bias is obtained by calculating the average value of the clock error's first difference with the reference AC of each satellite. The bias is then applied to the result from step (1) for each satellite, and we achieve an unbiased satellite clock error, which finally realizes the unification of the undifferenced satellite clock error time reference frame.

$$clk'''^s_{iepo,AC} = clk''^s_{iepo,AC} - \frac{\sum_{iepo=1}^n clk''^s_{iepo,AC} - clk^s_{iepo,REF}}{n_1} \quad (9)$$

where $clk'''^s_{iepo,AC}$ is the satellite clock error with a unified time reference frame; $clk''^s_{AC,iepo}$ is the detrended satellite clock error; and n_1 is the number of clock error epochs in an arc without outliers.

After performing the above steps, the undifferenced clock error of each AC can be regarded as 'clean'; the final clock error accuracy of the AC is then calculated by a difference with the reference AC, where the standard deviation (STD) is selected as the evaluation standard.

3. Accuracy Evaluation of SSR Products

Based on the orbit determination requirements of space-borne GPS, only the orbit and clock corrections of GPS will be discussed in this paper. Considering that the stability of the RTS product's data flow is affected by the reception software, network stability, and broadcast institutions, as shown in Table 1, we used the open-source software BNC to receive SSR products provided by 11 institutions for 10 days from the day of the year (DOY) 144 to 153 of 2022 in the same network environment. Among the 11 ACs, IGS provided 3 types of corrections; only the single-epoch solution is discussed in the following part and is referred to as IGS01.

Table 1. Real-time service (RTS) products from different analysis centers (ACs).

AC	Mount Point	Supported System	Interval for Orbit and Clock Corrections (s)
BKG	SSRA00BKG0	G	60, 5
CAS	SSRA00CAS0	GREC	5, 5
CNE	SSRA00CNE0	GREC	5, 5
DLR	SSRA00DLR0	GREC	30, 5
ESA	SSRA00ESA0	G	5, 5
GFZ	SSRA00GFZ0	GREC	5, 5
GMV	SSRA00GMV0	GRE	5, 5
IGS ¹	SSRA01IGS0	G	5, 5
	SSRA02IGS0	GR	60, 10
	SSRA03IGS0	GREC	60, 10
NRC	SSRA00NRC0	G	5, 5
SHA	SSRA00SHA0	GREC	5, 5
WHU	SSRA00WHU0	GREC	5, 5

¹ SSRA01IGS0 is a single-epoch solution; SSRA02IGS0 and SSRA03IGS0 are Kalman filter solutions.

In addition to their good accuracy, the high dynamic characteristics of LEO satellites also necessitate high requirements for the integrity and continuity of corrections. This section begins by addressing the integrity, continuity, and accuracy of RTS corrections during the experiment.

3.1. Integrity

SSR product integrity is defined as the ratio of the number of received products to all products for all satellites in all epochs. The integrity of the SSR correction products of 11 ACs was assessed. As shown in Figure 1, the integrity rate of most ACs reached more than 90%; GMV was the highest, with an average rate of 97%. In contrast, the product availability provided by CAS and NRC was demonstrably low and significantly fluctuated. Only 50% of IGS01 products were received in DOY 149; the reasons for this phenomenon may have involved the following two points: (1) the network was unstable, affecting the reception of products, and a few epochs were intensively lost; (2) the broadcaster did not broadcast all the corrections due to other additional factors.

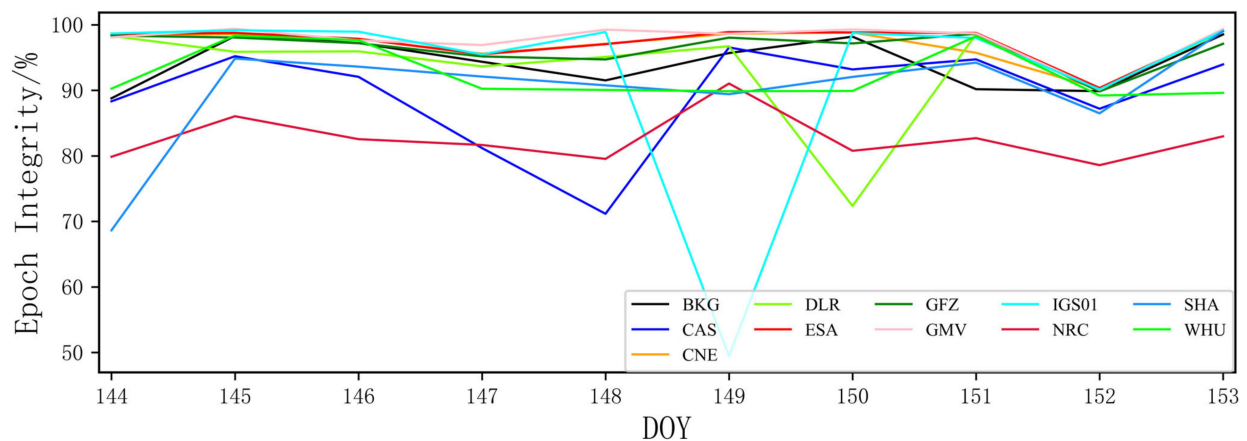


Figure 1. Integrity rate of State-Space Representation (SSR) products for all ACs.

3.2. Continuity

Figure 2 shows the product interruption of each AC during the experiment. According to the duration, the interruption was divided into the following intervals: (0, 5) min, (5, 10) min, (10, 30) min, (30, 120) min, and more than 120 min. The vertical axis is the number of interruptions corresponding with each interval. Among the ACs, the four in the first row had more interrupts in the (0, 5) min interval; thus, the longitudinal axis scale is enlarged relative to the other two lines. Especially for NRC, the number of interruptions at the (0, 5) min interval was as high as 1833, which meant that a small interruption occurred every 8 min on average. The small interruptions of the latter 7 ACs in the (0, 5) min interval remained below 200, showing good consistency. All ACs had a large interruption of more than 120 min; although this rarely occurred, it greatly affected the statistical results of the integrity rate detailed in Section 3.1. In general, the CNE, ESA, GMV, and IGS01 products had better continuity.

To show the distribution of interrupts more intuitively, a day was taken as an example for detailed research. Figure 3 shows the time series of the correction products of NRC on DOY 144 of 2022. On this day, there was a uniform small interruption every two hours. This was because, when the orbit correction was generated, the least squares method was generally used to predict the real-time orbit. The generated ultra-rapid orbit had poor accuracy at the prediction boundary, resulting in the discontinuity of the orbit correction product, which was expected to be solved by the filtering method [39,40]. Moreover, several satellites experienced simultaneous interrupts for several consecutive epochs, but such a continuous interruption was not regularly distributed. It must be pointed out that interruptions with a long duration (such as 1 h) posed significant challenges to the clock error fit and ultimately affected the application effect.

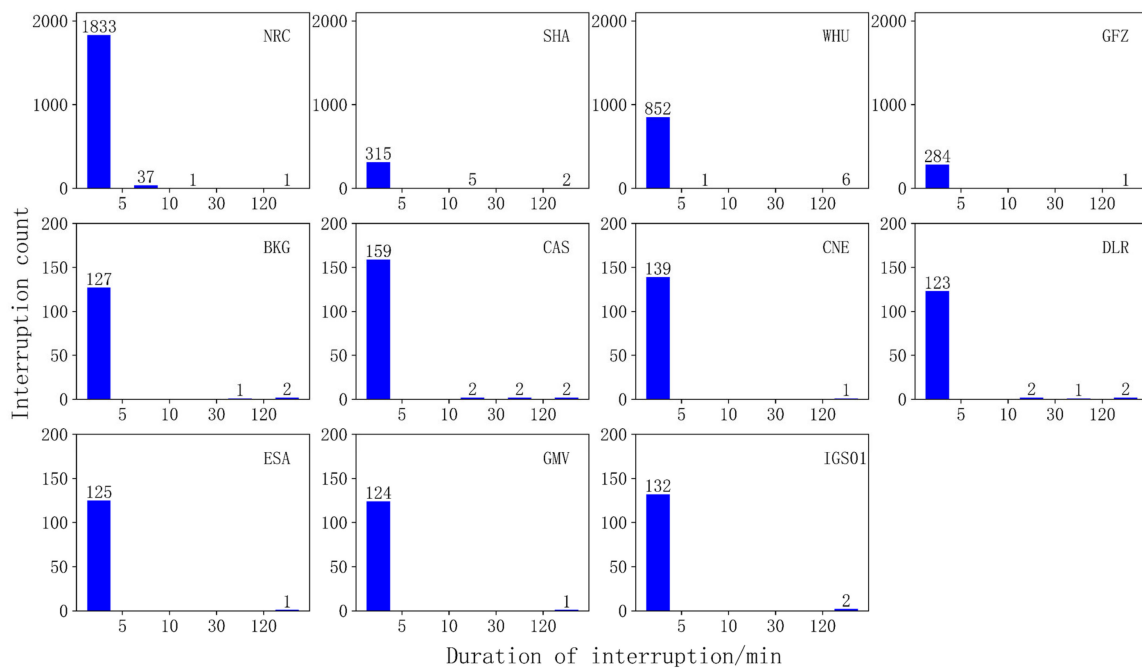


Figure 2. Histograms of the durations of interruptions.

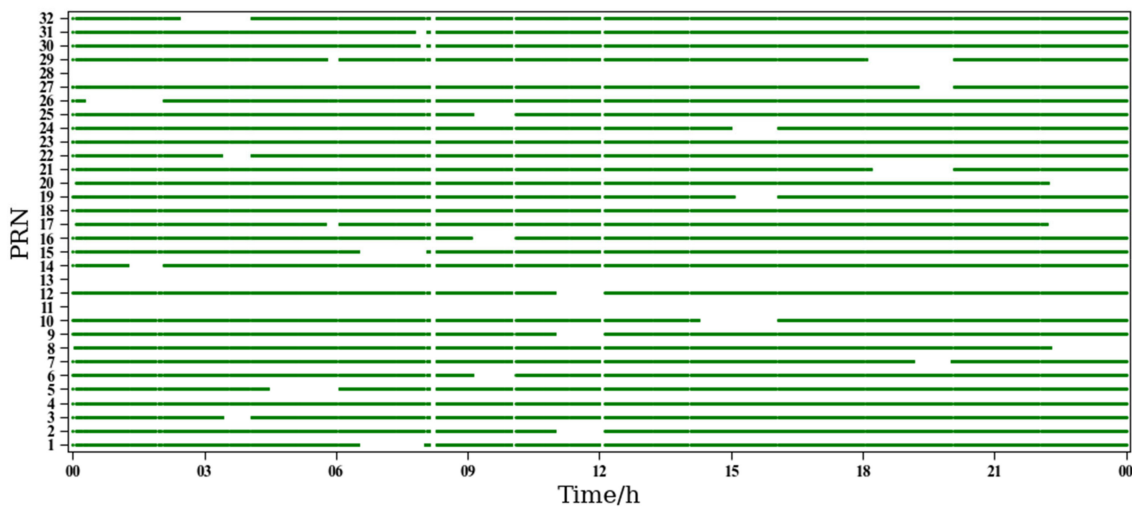


Figure 3. Time series of SSR correction from NRC on day of the year (DOY) 144 of 2022.

3.3. Accuracy

Based on the IGS final product, the accuracy of the RTS orbit and clock error during the experiment was evaluated. Users can quickly obtain the final product of IGS by accessing the website <https://cddis.nasa.gov/archive/gnss/products> (accessed on 24 May 2022) of the NASA data center Crustal Dynamic Data Information System (CDDIS) through a registered account.

3.3.1. Orbit Accuracy

The orbit difference is used to describe the accuracy of a satellite orbit. It refers to the comparison of the orbits calculated by different ACs at the same epoch. The accuracy is usually measured by the three-dimensional root mean square (3D-RMS), which was calculated as Formula (10). During the experiment, the PRN 28 satellite was not available and the PRN 11 satellite was only partially available. Moreover, PRN 08 and PRN 12 were

also missing for up to one day. The final 3D-RMS error was calculated by all available observation differences.

$$RMS = \sqrt{\frac{1}{m} \sum_{i=1}^m (x_{ac} - x_{ref})^2} \tag{10}$$

where the total number of epochs for the error analysis is denoted by m ; $x = [\delta x_r \ \delta x_a \ \delta x_c]^T$ is the satellite position in orbit coordinate system.

Figure 4 shows the RMS values of each GPS satellite from all ACs in the R, A, and C directions. In general, the RTS orbit accuracy of all ACs reached the centimeter level. The accuracy of different satellites in the same AC was generally consistent, but the overall performance considerably varied among the different ACs. Especially for SHA, the error in the radial direction greatly differed from the other two directions. This was because the radial accuracy of the GNSS orbit was generally stable whilst the along-track and cross-track directions were greatly affected by the dynamic model and observation numbers. It was noted that, for all ACs, the RMS of the PRN 11 and PRN 18 satellites was significantly larger than that of other satellites; this result may have been related to the maneuver characteristics of the satellites. In addition, no accuracy-related Block phenomenon was found in the orbit evaluation.

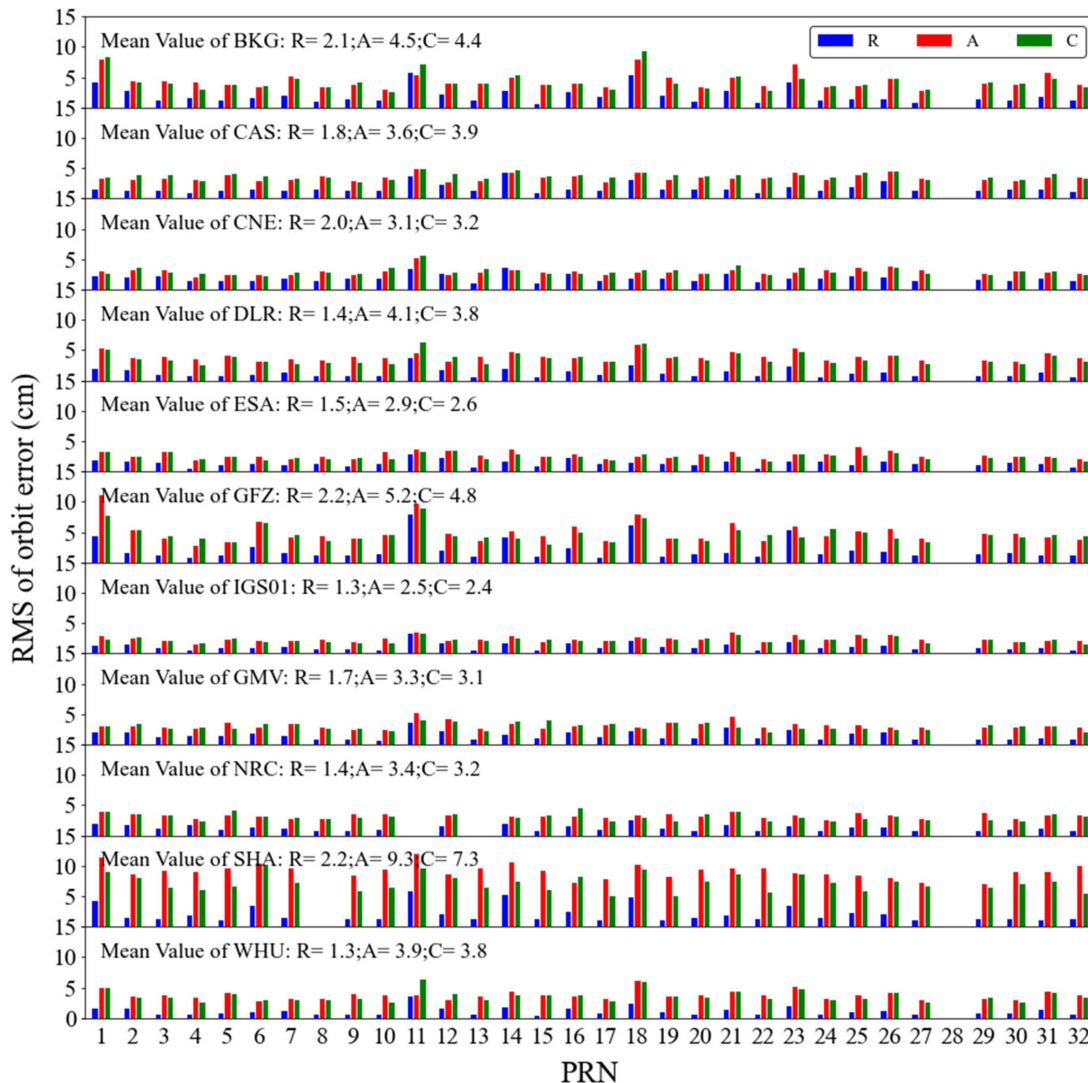


Figure 4. The root mean square (RMS) values in the radial (R), along-track (A), and cross-track (C) directions of GPS real-time orbits from different IGS ACs (the mean RMS of orbit errors for all GPS satellites is shown in each subplot).

3.3.2. Clock Error Accuracy

According to the evaluation method in Section 2.2, all satellite clock errors during the experiment were evaluated. Figure 5 shows the standard deviation (STD) of the GPS satellite clock errors from different ACs, which are arranged in the order of blocks, and the block updates are from left to right (Block IIR, Block IIR-M, Block IIF, and Block IIIA). Among the clock products of all the ACs, the WHU and CNES clock products were the best, with average STD values of 15.65 ps and 16.98 ps, respectively, whereas those of IGS01 and GMV were the worst, with average STD values of 30.92 ps and 29.81 ps, respectively. The real-time products of CNES are zero-difference integer ambiguity fixing solutions, whereas other ACs generally adopt floating solutions. This was the main reason why the CNES clock products were more accurate.

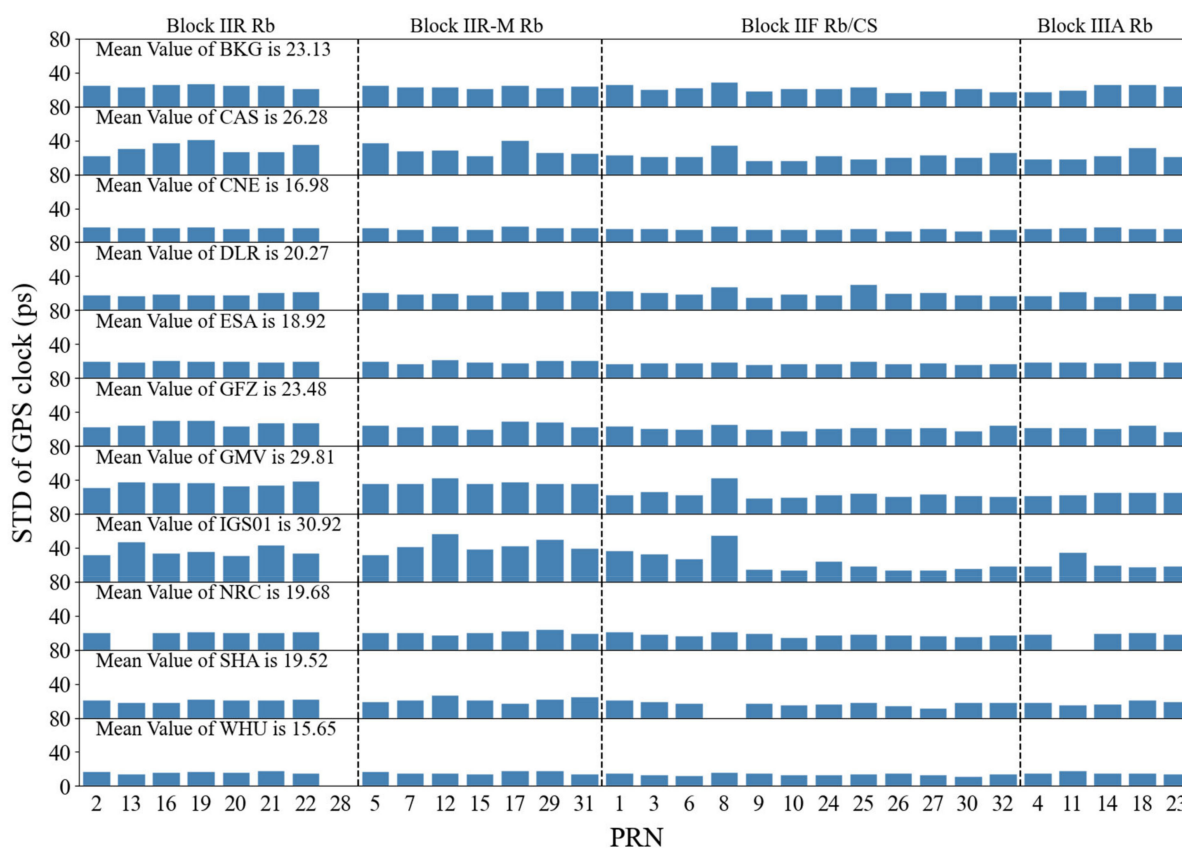


Figure 5. The standard deviations (STDs) of real-time GPS clock errors from different ACs (the mean STD of the clock errors for all GPS satellites is shown in each subplot).

What is more, there were obvious differences in clock performance between the satellites of the same AC, even within the same Block. At present, except for PRN 8 and PRN 24 (Block IIF in Figure 5), which use cesium atomic clocks, all GPS satellites starting from Block IIR are equipped with rubidium atomic clocks. It can be seen from Figure 5 that the clock accuracy of PRN 08 was slightly lower than that of other the satellites in Block IIF, which may have been related to the properties of the cesium atomic clock.

For demonstration purposes, the results of four representative satellites from the current four operational GPS blocks are shown in Figure 6: PRN 16 (a typical satellite from Block IIR), PRN 29 (Block IIR-M), PRN 30 (Block IIF), and PRN 14 (Block IIIA).

Furthermore, we listed the clock error STDs of different blocks for all ACs, as shown in Table 2, and averaged the same Block. The accuracy levels of Block IIR and Block IIR-M were close, with an average STD of about 25 ps, which was slightly worse than the value of 20 ps of Block IIF and Block IIIA. On the whole, we concluded that, with the modernization of GPS, the accuracy of satellite clocks has improved.

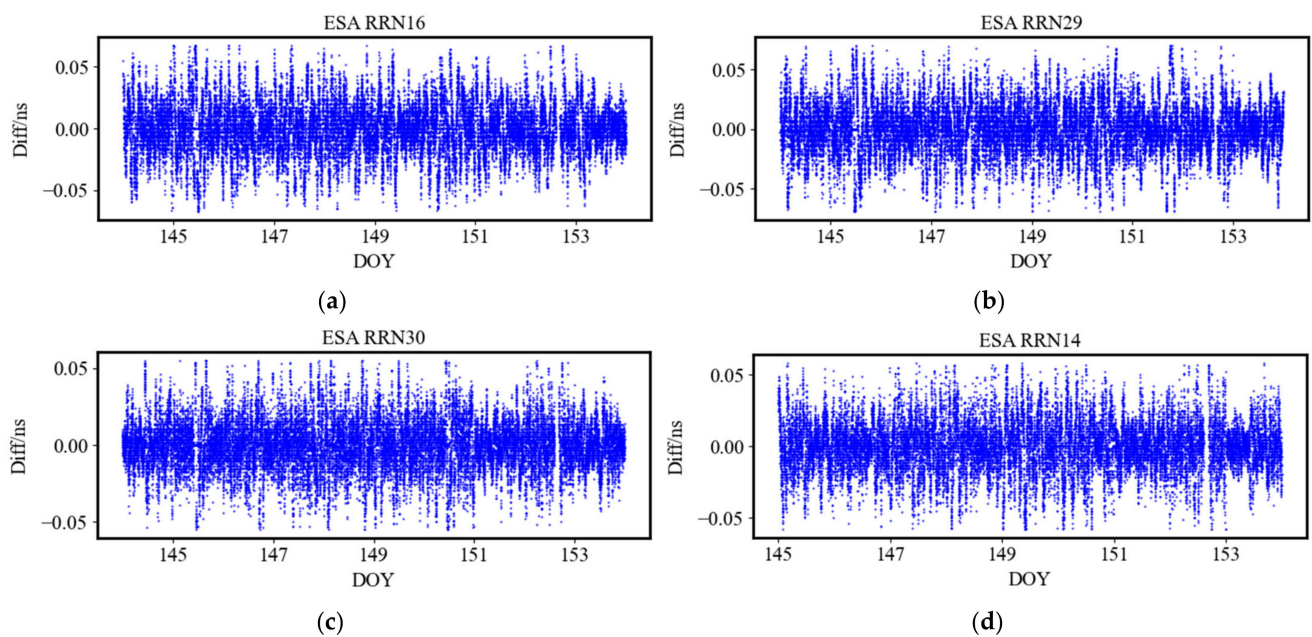


Figure 6. Scatterplots of IGS-RTS clock errors: PRN 16, Block IIR (a); PRN 29, Block IIR-M (b); PRN 30, Block IIF (c); and PRN 14, Block IIIA (d).

Table 2. Clock error STD arranged by Block (ps).

ACs	Block IIR	Block IIR-M	Block IIF	Block IIIA
BKG	25.02	23.88	21.67	22.96
CAS	31.89	30.08	22.26	22.77
CNE	17.86	17.66	16.03	17.05
DLR	19.34	20.93	21.09	18.65
ESA	19.8	19.89	17.79	19.03
GFZ	26.95	24.86	21.51	21.41
GMV	35.83	37.38	24.23	24.17
IGS01	36.94	43.16	23.9	22.19
NRC	21.13	20.93	18.22	19.70
SHA	20.88	22.19	17.42	18.47
WHU	16.75	16.59	14.36	15.91
Mean	24.76	25.23	19.86	20.21

4. Space-Borne POD Experiment and Accuracy Analysis

To evaluate the performance in terms of the orbit accuracy of LEO satellites based on the above RTS orbit and clock products, we performed reduced-dynamic and kinematic orbit determinations in the post-processing mode. The LEO satellite GRACE-C (GRCC) was selected as the research object, and the precise orbit ephemeris (POE) (FTP site isdftp.gfz-potsdam.de/grace-fo/Level-1B/JPL/INSTRUMENT/RL04, accessed on 24 May 2022) provided by JPL was used as the standard orbit to evaluate the orbit accuracy of this experiment. There was no obvious loss of space-borne data during the experiment period. Table 3 gives the model and description of the orbit determination.

Table 3. Strategies for low earth orbit satellite precise orbit determination.

Reference Frame	Description
Protocol inertial reference system Precession and nutation model Earth orientation parameter	Geocenter inertial reference system in J2000 IAU2000 R06 IERS C04
Dynamic model	Description
N-body gravity Gravity field of the earth Relativity effect Solid tide Ocean tide Radiation pressure	JPL DE421 GOCO06S IERS 2010 Conventions IERS 2010 Conventions FES2004 Empirical force model

Table 3. Cont.

Reference Frame	Description
Observation model	Description
Measurements	L3 P3 undifferenced ionosphere-free
Arc length and interval	24 h, 30 s
Cut-off elevation (°)	5
GPS satellite orbits and clocks	RTS-recovered products
Receiver antenna PCO/PCV	Pre-calibrated values
Parameter estimation	Description
Initial state	Initial position and velocity
Receiver clock error	Estimated as white noise, one bias per epoch
Ambiguity	Float solution
Pseudo-stochastic pulses	One group in the R, A, and C directions every 6 min

4.1. Reduced-Dynamic Precise Orbit Determination

The reduced-dynamic orbit determination of GRACE-C was carried out by using the strategy shown in Table 3 with the RTS-recovery GPS satellite orbit and clock errors. Figure 7 shows the RMS between the reduced-dynamic orbit results and the JPL orbit in the R, A, and C directions during the experiment. It can be seen from the figure that the space-borne GPS orbit results of all ACs achieved centimeter-level results by using the RTS-recovery orbit and clock products. Among the ACs, CNE, DLR, ESA, and IGS01 performed best, and the RMS error for three-dimensional position accuracy was about 3 cm. Meanwhile, the results of NRC were the worst, and the RMS in the R, A, and C directions was 2.8 cm, 3.9 cm, and 1.7 cm, respectively, which could be attributed to the poor integrity and continuity of the SSR product.

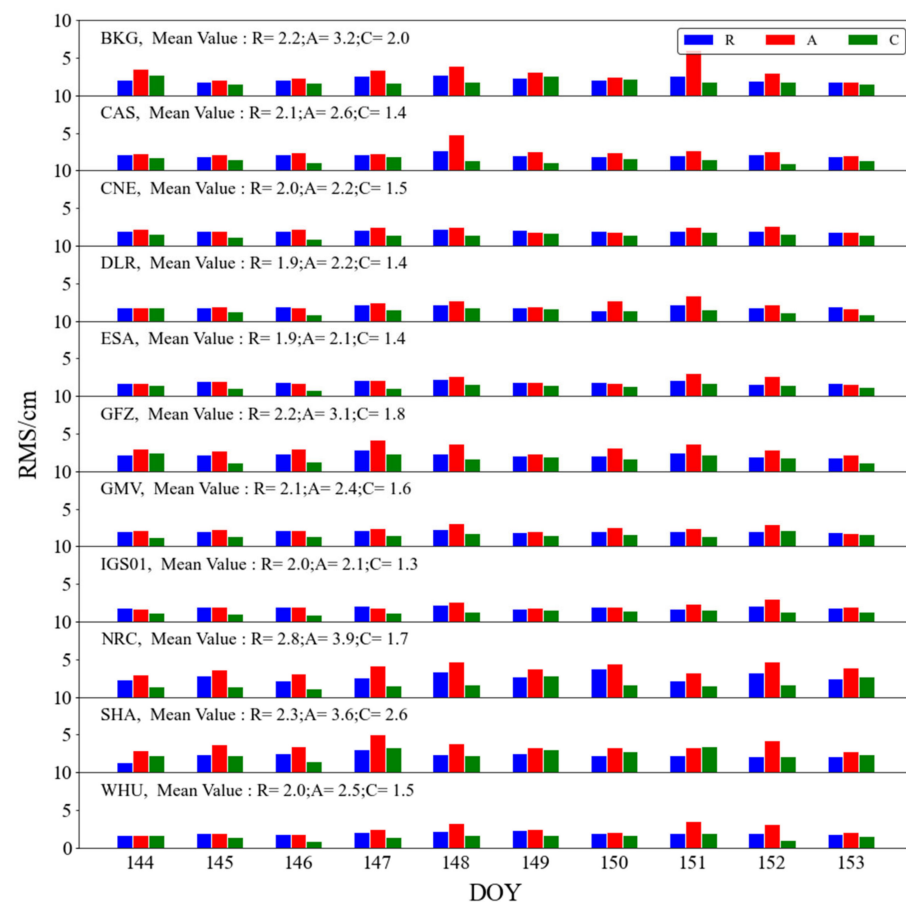


Figure 7. RMS of GRACE-C (GRCC) reduced-dynamic orbit products in the R, A, and C directions from JPL precise orbit ephemeris (POE) (the mean RMS of orbit errors for each AC is shown in each subplot).

4.2. Kinematic Precise Orbit Determination

Figure 8 shows the RMS of the kinematic orbit determination results and the JPL orbit during the experiment. As shown in Figure 8, the kinematic orbit accuracy of space-borne GPS also reached the centimeter level whilst considerably varying for the same AC on different dates; this result was positively correlated with the integrity and continuity of the SSR correction products. Due to the poor integrity and continuity of the NRC products, they did not participate in the kinematic orbit determination and the orbit evaluation results are not given in the figure. In addition, several results in the figure could not be fully displayed, which is further explained below.

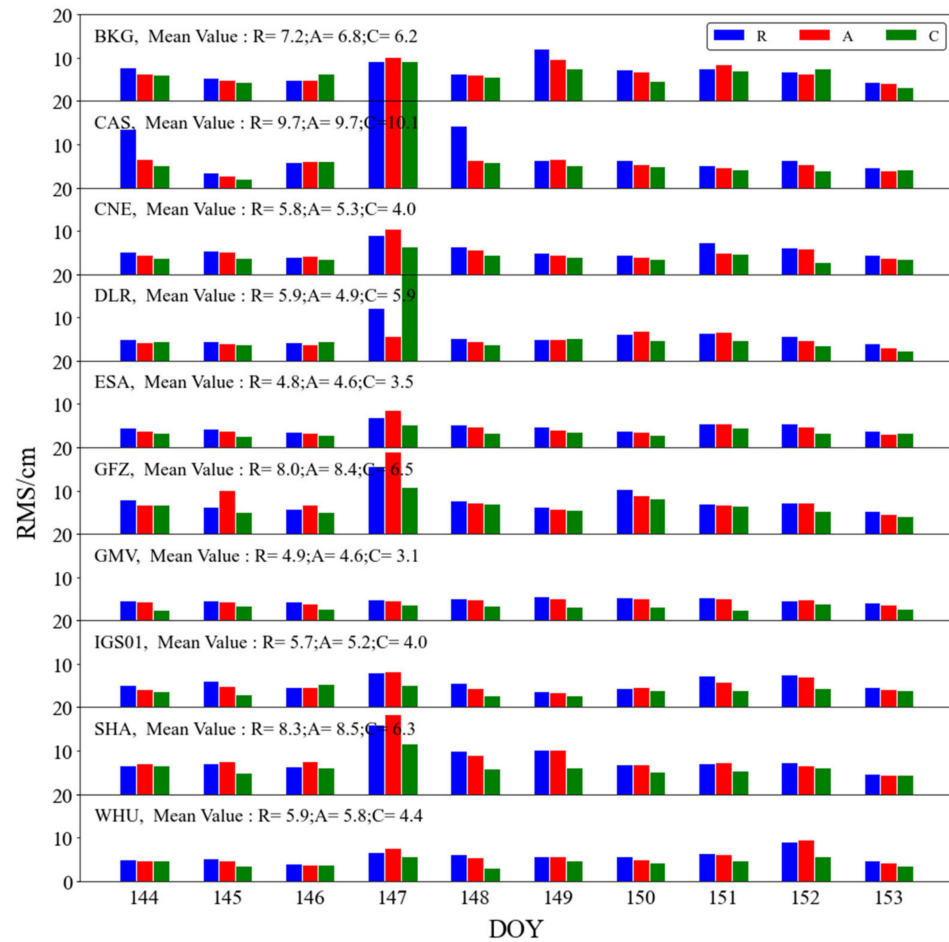


Figure 8. RMS of GRCC kinematic orbit products in the R, A, and C directions from JPL POE (the mean RMS of the orbit errors for each AC is shown in each subplot).

The orbit determination results of CAS and DLR on DOY 147 of 2022 were abnormal; Figure 9 shows the comparison results of the two ACs in the R, A, and C directions on this day. It can be seen from the figure that the comparison results jumped at a few epochs. Taking the previous analysis into account, it was found that there was a continuous lack of RTS products in these epochs. It was reasonable to infer that the long-term prediction of the clock error led to serious decay in accuracy, which indirectly produced inferior orbit results. This phenomenon also appeared in other cases with a serious lack of RTS products, and requires further research and solutions.

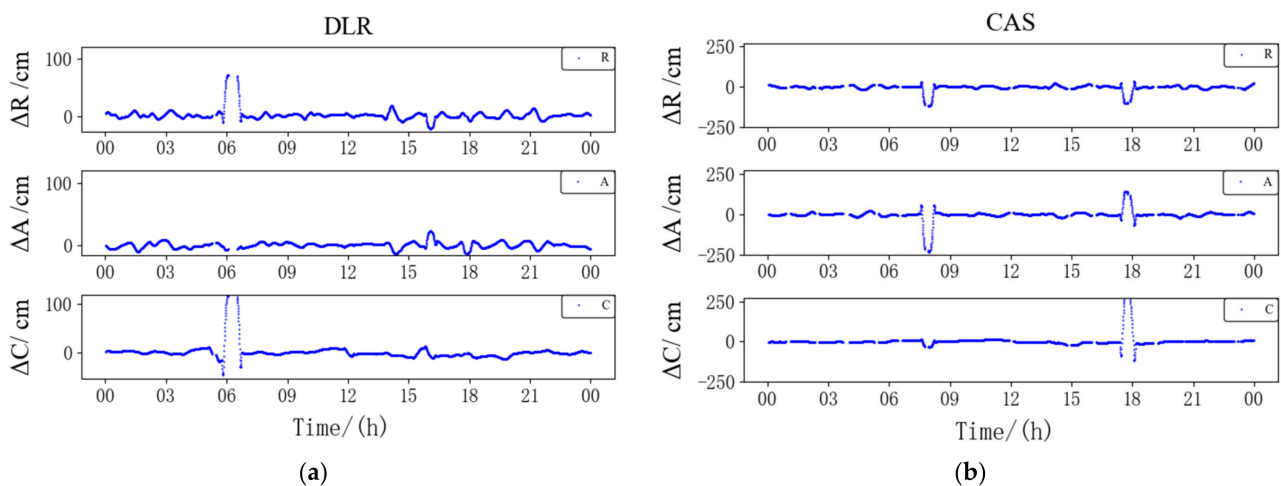


Figure 9. Orbit differences of GRCC kinematic results with JPL POE in the R, A, and C directions: (a) DLR result for DOY 147 of 2022; (b) CAS result for DOY 147 of 2022.

According to the comparison of the orbit determination results of the above two methods, we concluded that the reduced-dynamic method had lower requirements for the continuity of the product. Accordingly, the orbit results were more continuous and robust. Therefore, the reduced-dynamic method was suitable for generating ultra-rapid orbits of LEO satellites when using RTS products.

5. Conclusions

This paper has briefly introduced the background and application of RTS and elaborated on the recovery method of RTS orbit and clock errors. The integrity and continuity of real-time orbit and clock corrections provided by different ACs were discussed. Furthermore, we evaluated the RTS-recovery orbit and clock products. For clock error products in particular, an improved evaluation method was proposed and the accuracy of the RTS-recovery clock error products was given in more detail. Based on the RTS-recovery orbit and clock products from DOY 144 to DOY 153 of 2022, reduced-dynamic and kinematic orbit determinations of the GRACE-C satellite were carried out. Based on the above analysis, we present the following conclusions:

- (1) By studying the real-time orbit and clock correction products provided by 11 research institutions, including BKG, CAS, CNES, DLR, ESA, GFZ, GMV, IGS, NRC, SHA, and WHU, we concluded that the product integrity of BKG, CAS, and NRC needs to be improved, and the product continuity of NRC and WHU needs to be strengthened.
- (2) Compared with IGS final precise products, the numerical results showed that the RTS orbit accuracy of all ACs reached the centimeter level and the RMS in the radial direction was better than 0.02 m. Among the ACs, the orbit accuracy of IGS, SHA, and WHU was relatively high. The real-time clock error STD was 30 ps overall; WHU and CNES performed best, with STDs of 15.65 ps and 16.98 ps, respectively. In addition, the clock error accuracy was related to the Block. It was verified that the accuracy of Block IIR and Block IIR-M was slightly worse than that of Block IIF and Block IIIA.
- (3) Using RTS orbit and clock products, the radial accuracy of the GRACE-C space-borne GPS orbit determination based on the reduced-dynamic and kinematic methods reached the centimeter level and the average three-dimensional position accuracy values were 3.8 cm and 10.6 cm, respectively. As expected, the reduced-dynamic orbit was more robust and less affected by product integrity and continuity. It is advised that RTS products are used to carry out large-scale ultra-rapid orbit determinations for LEO satellites in the future.

It must be pointed out that the conclusions presented in this paper were based only on ten-day data from real-time products and the results can only be taken as a reference.

Data from a longer time span will be used for follow-up research, where space-borne observations from different LEO satellites will be collected for an analysis of the performance for ultra-rapid orbit determination.

Author Contributions: Proposal, K.L.; conceptualization, D.L. and X.Z.; methodology, D.L.; software, D.L.; validation, D.L.; writing—original draft, D.L.; writing—review and editing, D.L.; visualization, D.L.; supervision, X.Z. and K.L.; funding acquisition, K.L. All authors have read and agreed to the published version of the manuscript.

Funding: This research was funded by the National Natural Science Foundation of China (No. 12103077).

Data Availability Statement: The space-borne observations and the precise orbit ephemeris (POE) of LEO satellite GRACE-C (GRCC) are from FTP site isdcftp.gfz-potsdam.de/grace-fo/Level-1B/JPL/INSTRUMENT/RL04 (accessed on 24 May 2022).

Acknowledgments: The authors gratefully acknowledge the IGS Data Center of Wuhan University for the real-time data streams. We also acknowledge W.S. from Sun Yat-sen University for assisting in the early stage of the study.

Conflicts of Interest: The authors declare no conflict of interest.

References

1. Tapley, B.; Ries, J.C.; Davis, G.; Eanes, R.; Schultz, B.; Shum, C.K.; Watkins, M.; Marshall, J.; Nerem, R.; Putney, B. Precision Orbit Determination for TOPEX/Poseidon. *J. Geophys. Res. Atmos.* **1995**, *99*, 24383–24404. [[CrossRef](#)]
2. Kuang, D.; Bar-Sever, Y.; Bertiger, W.; Desai, S.; Haines, B.; Iijima, B.; Kruizinga, G.; Meehan, T.; Romans, L. Precise Orbit Determination for CHAMP Using GPS Data from BlackJack Receiver. In Proceedings of the 2001 National Technical Meeting of The Institute of Navigation, Long Beach, CA, USA, 24 January 2001; pp. 762–770.
3. Cerri, L.; Berthias, J.P.; Bertiger, W.I.; Haines, B.J.; Lemoine, F.G.; Mercier, F.; Ries, J.C.; Willis, P.; Zelensky, N.P.; Ziebart, M. Precision Orbit Determination Standards for the Jason Series of Altimeter Missions. *Mar. Geod.* **2010**, *33*, 379–418. [[CrossRef](#)]
4. Jäggi, A.; Hugentobler, U.; Bock, H.; Beutler, G. Precise Orbit Determination for GRACE Using Undifferenced or Doubly Differenced GPS Data. *Adv. Space Res.* **2007**, *39*, 1612–1619. [[CrossRef](#)]
5. Montenbruck, O.; Hackel, S.; Jäggi, A. Precise Orbit Determination of the Sentinel-3A Altimetry Satellite Using Ambiguity-Fixed GPS Carrier Phase Observations. *J. Geod.* **2018**, *92*, 711–726. [[CrossRef](#)]
6. Darugna, F.; Casotto, S.; Bardella, M.; Sciarratta, M.; Zoccarato, P. Sub-Decimeter Onboard Orbit Determination of LEO Satellites Using SSR Corrections: A Galileo-Based Case Study for the Sentinel-6A Satellite. *Remote Sens.* **2022**, *14*, 6121. [[CrossRef](#)]
7. Li, K.; Zhou, X.; Wang, W.; Gao, Y.; Zhao, G.; Tao, E.; Xu, K. Centimeter-Level Orbit Determination for TG02 Spacelab Using Onboard GNSS Data. *Sensors* **2018**, *18*, 2671. [[CrossRef](#)] [[PubMed](#)]
8. Mao, X.; Arnold, D.; Girardin, V.; Villiger, A.; Jäggi, A. Dynamic GPS-Based LEO Orbit Determination with 1 Cm Precision Using the Bernese GNSS Software. *Adv. Space Res.* **2020**, *67*, 788–805. [[CrossRef](#)]
9. Van den IJssel, J.; Encarnação, J.; Doornbos, E.; Visser, P. Precise Science Orbits for the Swarm Satellite Constellation. *Adv. Space Res.* **2015**, *56*, 1042–1055. [[CrossRef](#)]
10. Allahviridi-Zadeh, A.; El-Mowafy, A. Precise Orbit Determination of CubeSats Using a Proposed Observations Weighting Model. In Proceedings of the Scientific Assembly of the International Association of Geodesy (IAG), Beijing, China, 28 June 2021.
11. Caissy, M.; Agrotis, L.; Weber, G.; Fisher, S. The IGS Real-Time Service. In Proceedings of the EGU General Assembly Conference Abstracts 2013, Vienna, Austria, 7–12 April 2013.
12. Agrotis, L.; Caissy, M.; Ruelke, A.; Fisher, S. Real-Time Service Technical Report 2014. In *IGS Technical Report 2014*; IGS Central Bureau: Pasadena, CA, USA, 2014.
13. Rülke, A.; Agrotis, L. IGS Realtime Service Technical Report 2016. In *IGS Technical Report 2016*; IGS Central Bureau: Pasadena, CA, USA, 2016.
14. Weber, G.; Mervart, L.; Stürze, A.; Rülke, A.; Stcker, D. *BKG Ntrip Client (BNC)*; Version 2.12; Mitteilungen des Bundesamtes für Kartographie und Geodäsie: Frankfurt, Germany, 2016.
15. Takasu, T. *An Open Source Program Package for Gns Positioning*; RTKLIB: Hokuto, Japan, 2013.
16. Zhang, Y. Research on Real-Time High Precision BeiDou Positioning Service System. *Acta Geod. Cartogr. Sin.* **2018**, *47*, 1293.
17. Tegeedor, J.; Lapucha, D.; Melgrd, T.E.; Vigen, E.; Strandli, R. The New G4: Multi-Constellation Precise Point Positioning Using GPS, Glonass, Galileo and BeiDou. In Proceedings of the ION GNSS+ 2015, Tampa, FL, USA, 14–18 September 2015.
18. Jokinen, A.; Ellum, C.; Neumann, J.; Chan, D.; Morley, T. Kinematic Performance of NovAtel CORRECT with Terrastar-D Precise Point Positioning (PPP) Service. In Proceedings of the 27th International Technical Meeting of The Satellite Division of the Institute of Navigation (ION GNSS 2014), Tampa, FL, USA, 8–12 September 2014.
19. Dixon, K. StarFire: A Global SBAS for Sub-Decimeter Precise Point Positioning. In Proceedings of the International Technical Meeting of the Satellite Division of the Institute of Navigation 2006, Fort Worth, TX, USA, 26–29 September 2006.

20. Miya, M.; Fujita, S.; Sato, Y.; Ota, K.; Takiguchi, J. Centimeter Level Augmentation Service (CLAS) in Japanese Quasi-Zenith Satellite System, Its User Interface, Detailed Design, and Plan. In Proceedings of the 29th International Technical Meeting of The Satellite Division of the Institute of Navigation (ION GNSS+ 2016), Portland, OR, USA, 12–16 September 2016.
21. Pintor, P.; González, E.; Senado, A.; Bohlig, P.; Sperl, A.; Henkel, P.; Simón, J.; Hernández, C.; de Blas, J.; Vázquez, J. Galileo High Accuracy Service (HAS) Algorithm and Receiver Development and Testing. In Proceedings of the 35th International Technical Meeting of the Satellite Division of The Institute of Navigation (ION GNSS+ 2022), Denver, CO, USA, 19–23 September 2022.
22. Xu, Y.; Yang, Y.; Li, J. Performance Evaluation of BDS-3 PPP-B2b Precise Point Positioning Service. *GPS Solut.* **2021**, *25*, 142. [[CrossRef](#)]
23. Barrios, J.; Caro, J.; Calle, J.D.; Carbonell, E.; Pericacho, J.G.; Fernández, G.; Esteban, V.M.; Fernández, M.A.; Bravo, F.; Torres, B.; et al. Update on Australia and New Zealand DFMC SBAS and PPP System Results. In Proceedings of the 31st International Technical Meeting of the Satellite Division of The Institute of Navigation (ION GNSS+ 2018), Miami, FL, USA, 24–28 September 2018.
24. Li, B.; Ge, H.; Bu, Y.; Zheng, Y.; Yuan, L. Comprehensive Assessment of Real-Time Precise Products from IGS Analysis Centers. *Satell. Navig.* **2022**, *3*, 12. [[CrossRef](#)]
25. Alcay, S.; Turgut, M. Evaluation of the Positioning Performance of Multi-GNSS RT-PPP Method. *Arab. J. Geosci.* **2021**, *14*, 155. [[CrossRef](#)]
26. Yu, C.; Zhang, Y.; Chen, J.; Chen, Q.; Xu, K.; Wang, B. Performance Assessment of Multi-GNSS Real-Time Products from Various Analysis Centers. *Remote Sens.* **2022**, *15*, 140. [[CrossRef](#)]
27. Kazmierski, K.; Sońnica, K.; Hadas, T. Quality Assessment of Multi-GNSS Orbits and Clocks for Real-Time Precise Point Positioning. *GPS Solut.* **2017**, *22*, 11.
28. Elsobeiey, M.; Al-Harbi, S. Performance of Real-Time Precise Point Positioning Using IGS Real-Time Service. *GPS Solut.* **2016**, *20*, 565–571. [[CrossRef](#)]
29. Zhiyu, W.; Zishen, L.; Liang, W.; Xiaoming, W.; Hong, Y. Assessment of Multiple GNSS Real-Time SSR Products from Different Analysis Centers. *ISPRS Int. J. Geo-Inf.* **2018**, *7*, 85.
30. Wang, Z.; Li, Z.; Wang, L.; Wang, N.; Yang, Y.; Li, R.; Zhang, Y.; Liu, A.; Yuan, H.; Hoque, M. Comparison of the Real-Time Precise Orbit Determination for LEO between Kinematic and Reduced-Dynamic Modes. *Measurement* **2022**, *187*, 110224. [[CrossRef](#)]
31. Wang, Z.; Li, Z.; Wang, N.; Hoque, M.; Wang, L.; Li, R.; Zhang, Y.; Yuan, H. Real-Time Precise Orbit Determination for LEO between Kinematic and Reduced-Dynamic with Ambiguity Resolution. *Aerospace* **2022**, *9*, 25. [[CrossRef](#)]
32. Giordano, P.; Zoccarato, P.; Otten, M.; Crisci, M. P2OD: Real-Time Precise Onboard Orbit Determination for LEO Satellites. In Proceedings of the 30th International Technical Meeting of The Satellite Division of the Institute of Navigation (ION GNSS+ 2017), Portland, OR, USA, 25–29 September 2017.
33. El-Mowafy, A.; Deo, M.; Kubo, N. Maintaining Real-Time Precise Point Positioning during Outages of Orbit and Clock Corrections. *GPS Solut.* **2017**, *21*, 937–947. [[CrossRef](#)]
34. Hauschild, A.; Tegedor, J.; Montenbruck, O.; Visser, H.; Markgraf, M. Precise Onboard Orbit Determination for LEO Satellites with Real-Time Orbit and Clock Corrections. In Proceedings of the 29th International Technical Meeting of The Satellite Division of the Institute of Navigation (ION GNSS+ 2016), Portland, OR, USA, 12–16 September 2016.
35. El-Mowafy; Ahmed Real-Time Precise Point Positioning Using Orbit and Clock Corrections as Quasi-Observations for Improved Detection of Faults. *J. Navig.* **2018**, *71*, 769–787. [[CrossRef](#)]
36. Svehla, D.; Rothacher, M. Kinematic and Reduced-Dynamic Precise Orbit Determination of Low Earth Orbiters. *Adv. Geosci.* **2003**, *1*, 47–56. [[CrossRef](#)]
37. Wu, S.C.; Yunck, T.P.; Thornton, C.L. Reduced-Dynamic Technique for Precise Orbit Determination of Low Earth Satellites. *J. Guid. Control Dyn.* **2012**, *14*, 24–30. [[CrossRef](#)]
38. Kouba, J.; Springer, T. New IGS Station and Satellite Clock Combination. *GPS Solut.* **2001**, *4*, 31–36. [[CrossRef](#)]
39. Dai, X.; Gong, X.; Li, C.; Qing, Y.; Gu, S.; Lou, Y. Real-Time Precise Orbit and Clock Estimation of Multi-GNSS Satellites with Undifferenced Ambiguity Resolution. *J. Geod.* **2022**, *96*, 73. [[CrossRef](#)]
40. Tan, B.; Yuan, Y.; Ai, Q.; Zha, J. Real-Time Multi-GNSS Precise Orbit Determination Based on the Hourly Updated Ultra-Rapid Orbit Prediction Method. *Remote Sens.* **2022**, *14*, 4412. [[CrossRef](#)]

Disclaimer/Publisher’s Note: The statements, opinions and data contained in all publications are solely those of the individual author(s) and contributor(s) and not of MDPI and/or the editor(s). MDPI and/or the editor(s) disclaim responsibility for any injury to people or property resulting from any ideas, methods, instructions or products referred to in the content.